Surface & Coatings Technology 477 (2024) 130295

Contents lists available at ScienceDirect

Surface & Coatings Technology

journal homepage: www.elsevier.com/locate/surfcoat

Surface characteristics and tribological behavior of 3D-printed 316 L steel after plasma assisted low temperature carburizing

E. Bolli [a], S. Kaciulis [a], A. Lanzutti [b,*], A. Mezzi [a], R. Montanari [c], A. Palombi [c], F. Sordetti [b], E. Vaglio [b], A. Varone [c,*], C. Verona [c]

[a] ISMN-CNR, P.O. Box 10, 00015 Monterotondo Stazione, Rome, Italy
[b] Polytechnic Department of Engineering and Architecture, University of Udine, Via delle Scienze 208, 33100 Udine, Italy
[c] Department of Industrial Engineering, University of Rome "Tor Vergata", Via del Politecnico 1, 00133 Roma, Italy

ARTICLE INFO

Keywords:
316L steel
Laser powder bed fusion
Plasma assisted low temperature carburizing
Wear
XRD
Raman
XPS

ABSTRACT

Conventional carburizing treatments of steels are usually carried out above 550 °C thus they are not suitable for austenitic stainless steels because surface hardening is achieved to detriment of corrosion resistance. To overcome this drawback different carburizing treatments at lower temperature have been developed and among them one of the most efficient is a plasma assisted process at 475 °C. With respect to austenitic stainless steels produced through traditional processes additive manufacturing allows to obtain mechanical parts of complex shape with enhanced strength and without loss of ductility. However, for certain applications the components still suffer of limited hardness and wear resistance. In this work the plasma assisted process at 475 °C has been employed to treat the 316 L steel manufactured by Laser Powder Bed Fusion (L-PBF) with the aim of improving its tribological behavior. The treatment time was 7 h and gas mixtures ($CH_4 + H_2$) with different amounts of CH_4 have been used. The samples were then submitted to wear tests in pin-on-flat (POF) mode at room temperature with applied loads of 10 N and 20 N. The surface characteristics were examined by scanning electron microscopy (SEM), atomic force microscopy (AFM), X-ray diffraction (XRD), Raman spectroscopy (RS), glow discharge optical emission spectroscopy (Rf-GDOES), and X-ray photoelectron spectroscopy (XPS). The results show that plasma treatments induce the formation of a ~ 25 μm thick layer of expanded austenite (S-phase) that is covered by a diamond like carbon (DLC) over-layer of ~2 μm. Such over-layer exhibits a complex sub-structure: the inner part consists of amorphous C (sp^2 bonds) with a degree of topological disorder depending on the gas mixture whereas in the external part both sp^2 (graphite-like) and sp^3 (diamond-like) bonds are present with relative amounts changing with the distance from the surface. Independently on the gas mixture used in plasma treatment, all the samples exhibit a wear resistance much better than that of the untreated material. Moreover, wear resistance also depends on plasma treatment conditions: the greater the CH_4 content, the lower the wear resistance. The results have been discussed by considering the intrinsic DLC brittleness that fractures and detaches from the metal surface during the tests thus hard debris take part to the wear process acting as abrasive particles.

1. Introduction

Austenitic stainless steels are used today in several industrial sectors (chemical, energy, biomedical, pharmaceutical, etc.) due to their excellent corrosion resistance and toughness [1]. However, an intrinsic limit to their applications is represented by low hardness and wear resistance that may lead to galling, scoring and seizure of mechanical parts [2]. Conventional thermo-chemical surface treatments (carburizing, nitriding and carbo-nitriding) are usually performed at temperature (above 550 °C) where precipitation of Cr carbides occurs with Cr depletion of the surrounding matrix. Therefore, they are not suitable for austenitic stainless steels because surface hardening is achieved to detriment of corrosion resistance.

To overcome these drawbacks different thermo-chemical treatments at lower temperature (350–550 °C) have been developed and among them one of the most efficient consists of two steps [3]: (i) Cr_2O_3 is

* Corresponding authors.
E-mail addresses: alex.lanzutti@uniud.it (A. Lanzutti), alessandra.varone@uniroma2.it (A. Varone).

https://doi.org/10.1016/j.surfcoat.2023.130295
Received 28 September 2023; Received in revised form 20 November 2023; Accepted 10 December 2023
Available online 15 December 2023

Table 1
Surface hardness of the as-built and plasma treated 316 L steel with different CH_4 content in the gas mixture.

CH_4 content	Not treated	0.5 %	1.0 %	2.0 %	2.5 %	4.0 %
Hardness HV_1	245 ± 3	450 ± 13	467 ± 10	534 ± 36	547 ± 27	421 ± 21

removed from the steel surface by means of a pre-treatment in gaseous HCl at ~250 °C, (ii) the material is treated at ~450 °C for about 30 h in an atmosphere of CO, H_2 and N_2. The result is a surface layer of expanded austenite (S-phase), supersaturated of C, that exhibits higher hardness [3] and Young's modulus [4,5] than those of austenite and also improved corrosion resistance [6–8]. Other important characteristics of the hardened layer are its good ductility due to the f.c.c. structure [9] and the presence of surface compressive residual stresses (up to 2 GPa) which contribute to improve fatigue resistance [10,11]. Wear resistance is remarkably enhanced too [12–15], also at temperature up to 600 °C [16].

A serious drawback is the long treatment time involving high costs, therefore a plasma assisted carburizing process at low temperature has been developed [17–20]. By exploiting the chemical reactivity of the ionized gas and its collision energy, such treatment produces similar effects but in shorter time (~7 h). Plasma treatments on austenitic stainless steels were also performed by Gobbi et al. [21], Liu et al. [22,23] and Savrai et al. [24] with general improvement of mechanical properties and corrosion resistance.

In the last decade, additive manufacturing is gaining increasing interest to produce mechanical parts made of austenitic stainless steels. In fact, this process achieves significant strengthening without loss of ductility of the steel, thanks to the formation of a microstructure consisting of dendrite walls made of dislocations pinned by nano-oxides [25–31]. The mechanical properties are better than those of the same wrought and cast materials. However, the tribological properties of the additively manufactured steels are not sufficient for components where a tribocontact is present, e.g. in industrial food processing. To increase the wear resistance of the material, surface treatments are also necessary. Recently, carburizing at low temperature of 3D-printed stainless austenitic steels was performed by Yang et al. [32] and Funch et al. [33]. Indeed, the plasma assisted carburizing process at low temperature was carried out by us [34] to harden the surface of 316 L steel manufactured by laser powder bed fusion (L-PBF). Among austenitic stainless steels 316 L is one of the most used in industrial applications due to its excellent corrosion resistance, therefore it was chosen for present experiments. Plasma treatments were performed at 475 °C for 7 h by using various gas mixtures with different amounts of H_2, CH_4 and CO_2. The results showed that the gas mixtures consisting of $CH_4 + H_2$ were the most effective leading in some cases to a surface hardness more than double than that of the original material (see Table 1). Moreover, it was observed that in all the samples the S-phase is always covered by a thin and very hard over-layer rich of C.

This work was carried out to investigate the tribological behavior of 316 L steel manufactured by L-PBF and submitted to plasma treatments with gas mixtures containing different amounts of CH_4. The results have been discussed on the basis of surface characteristics investigated by X-ray diffraction (XRD), Raman spectroscopy (RS), scanning electron microscopy (SEM), atomic force microscopy (AFM), glow discharge optical emission spectroscopy (Rf-GDOES), and X-ray photoelectron spectroscopy (XPS) with depth profiling. From the XPS depth profiles the chemical composition of C-rich over-layer has been determined, while the C electronic configuration has been identified from the values of D parameter, calculated from C KLL spectra.

2. Materials and methods

2.1. Sample preparation

The plasma assisted low temperature carburizing treatments were performed on 316 L steel produced by L-PBF. The raw metal powder used for producing the samples consisted of spherical particles ranging from d_{10} = 18.17 μm to d_{90} = 45.44 μm in diameter, and had the chemical composition reported in Table 2.

The samples were manufactured on a Concept Laser M2 Cusing machine equipped with a single-mode CW ytterbium-doped fiber laser, whose emission wavelength is 1070 nm. The process was performed under inert Ar atmosphere with a residual O <0.2 %. A total of 20 rectangular blocks (30.5 × 20.5 × 7 mm^3) were built with the major surfaces parallel to the building platform (Fig. 1). The main L-PBF process parameters were the following: laser power $P = 180$ W, scanning speed v_s = 600 mm/s, laser spot diameter d_l = 120 μm, hatch distance h_d = 105 μm, layer thickness t_l = 25 μm. The exposure was executed dividing each layer into 5 × 5 mm^2 squares that were scanned according to the same bi-directional, alternated and rotated pattern described in [34]. The structure of the obtained steel consists of austenite plus ~5 % of δ-ferrite (maximum content).

The produced blocks were then separated from the building platform and cut parallel to the minor lateral surfaces by using a diamond saw to obtain firstly 2 mm thick slices and subsequently 7 × 6 × 2 mm^3 bricks used for the experiments. Before undergoing plasma treatments, the samples were mechanically polished by using grinding papers and finally a suspension of 0.3 μm alumina powder in water to obtain a mirror-like surface (Ra = 0.1 μm), and immersed in a sonication bath for 10 min.

2.2. Plasma treatments

Plasma treatments on the surface of 316 L steel were performed by using a microwave plasma enhanced chemical vapour deposition (CVD) reactor [35]. A schematic view of the experimental set-up is shown in

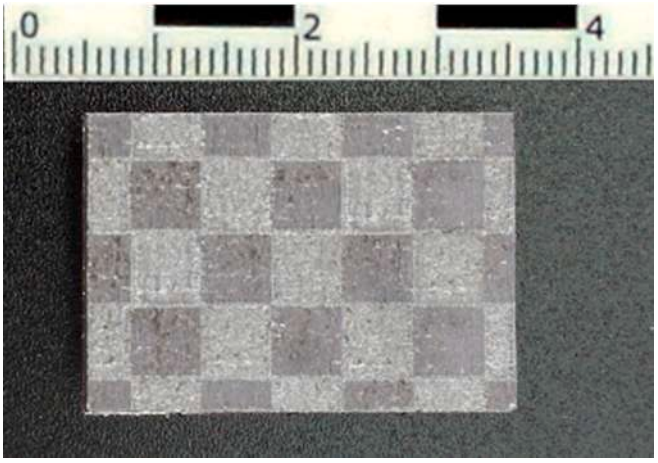

Fig. 1. Rectangular block produced by L-PBF.

Table 2
Nominal chemical composition (wt%) of the 316 L steel powders used to manufacture the samples by L-PBF.

C	Cr	Mo	N	Mn	Si	Ni	P	S	Fe
0.024	16.87	2.06	0.083	1.35	0.40	10.05	0.031	0.029	to balance

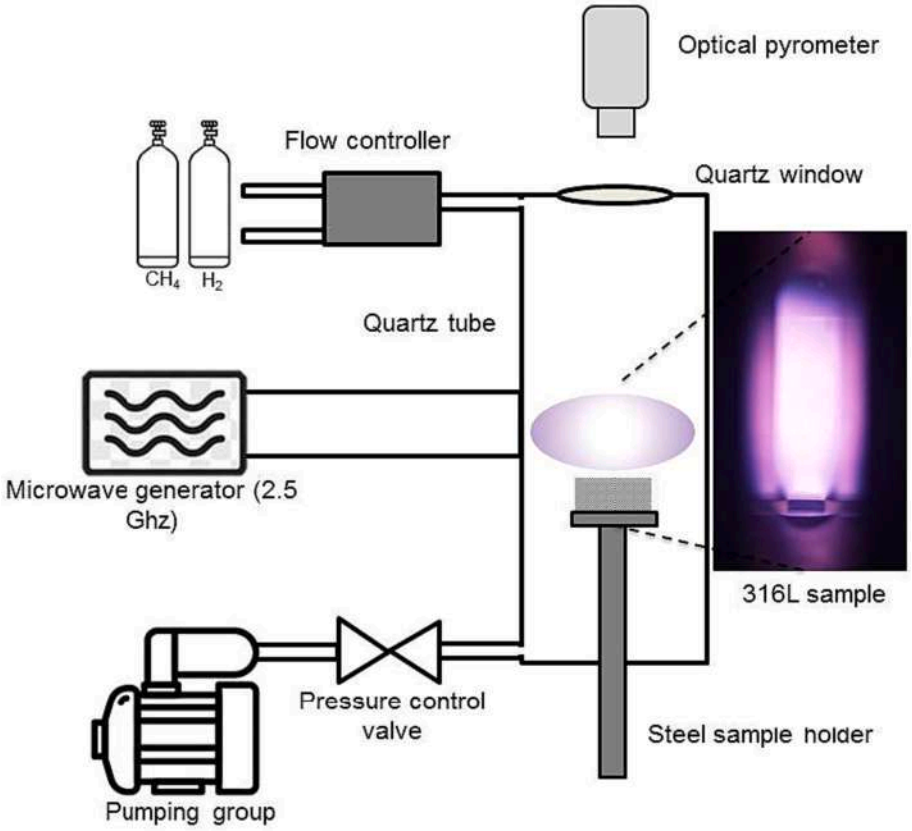

Fig. 2. Schematic view of the experimental set-up used for plasma treatments.

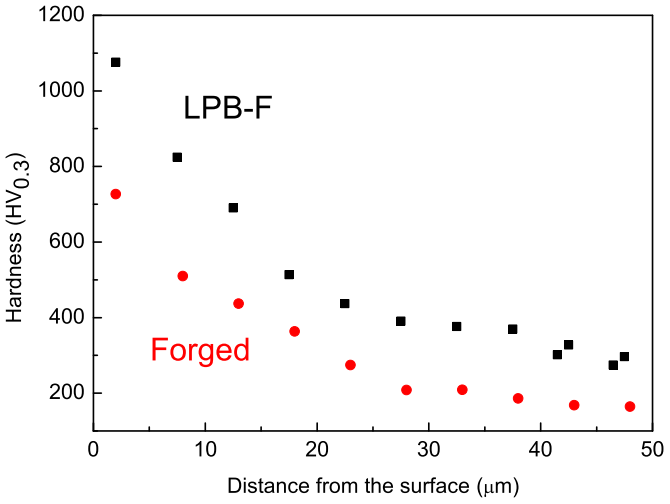

Fig. 3. Hardness vs. distance from the surface measured on cross-sections of LPB-F and forged 316 L steel after plasma treatments with 2 % of CH_4 in the gas mixture.

Fig. 2. Before the plasma treatments, a hydrogen bombardment (for 15 min in the same reactor) was carried out on the sample surface to remove the passive oxidation layer.

High purity gases, such as H_2 and CH_4 were introduced in the vacuum chamber of the CVD reactor, after that a background pressure of the order of 10^{-5} mbar was achieved. The pressure in the chamber was fixed to about 70 mbar and the microwave power was varied in the range 400–500 W to have a temperature of about 475 °C. Such temperature was chosen to avoid the precipitation of $M_{23}C_6$ carbides and other undesired phases (η, χ and σ) [3]. From the TTT diagram reported in a previous work [34] the time necessary for the formation of $M_{23}C_6$ carbides at 475 °C exceeds 10^4 h, a time much longer than that of our treatments (7 h). This is confirmed by SEM observations.

The samples were treated by using different gas mixtures of methane and hydrogen. In particular, the CH_4 concentration in the gas mixture was 0.5 %,1 %, 2 %, 2.5 % and 4 % diluted in H_2 at a total flow of 100 sccm.

2.3. Sample characterization

The surface morphology of plasma treated samples has been investigated by field emission scanning electron microscopy (FE-SEM- Zeiss Leo Supra 35, Germany).

To determine the thickness of the modified surface layer, cross-sections of the samples have been examined by light microscopy (LM-microscope Union Optical Co., Ltd., Tokyo, Japan) after mechanical polishing by means of grit papers and diamond paste up to 1 μm, and chemical etching with Beraha II reagent.

XRD measurements were performed by using a PW 1729 diffractometer (Philips, Eindhoven, The Netherlands) with Mo-Kα radiation (λ = 0.07093 nm). Precision peak profiles of the most intense reflections have been recorded with 2θ steps of 0.005° and counting time of 10 s per step. Lattice parameters of the untreated austenite ($a_{0\gamma}$) and S-phase (a_γ) have been determined by using the $\cos^2\theta$ method [36] and from these values the C content C_γ (wt%) in the S-phase has been then calculated through the empirical relationship proposed by Ridley et al. [37]:

$$a_\gamma = a_{0\gamma} + \alpha C_\gamma \quad (1)$$

being the constant α = 0.0044 nm/wt% C.

Glow discharge optical emission spectroscopy (Rf-GDOES) was used to measure the C profile vs. surface distance in the modified layers. The

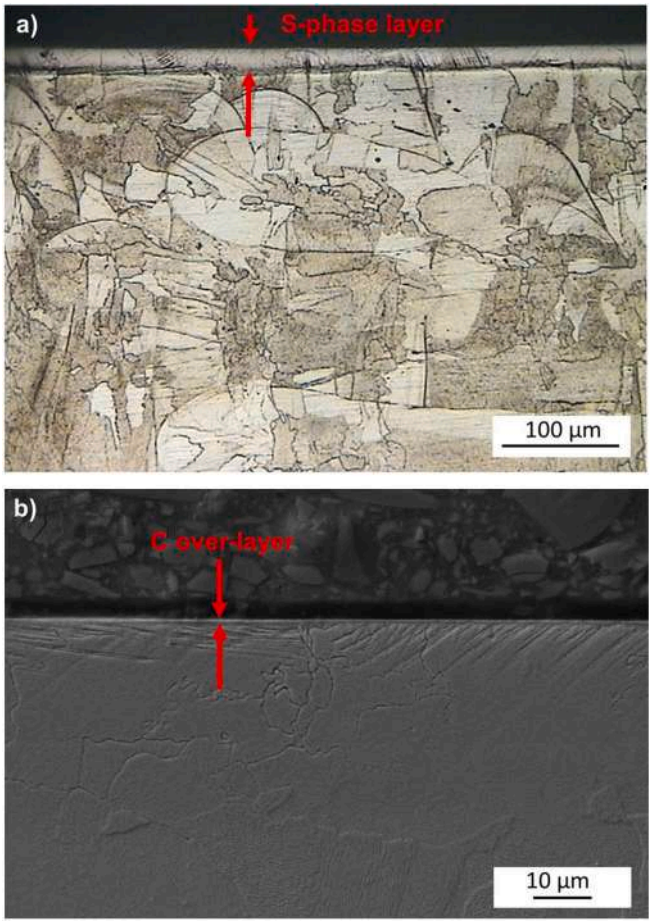

Fig. 4. Cross-section of a sample plasma treated with 2.5 CH_4 + 97.5 H_2 showing the S-phase layer covering the plasma exposed surface (a). At higher magnification the C over-layer is observed (b).

measurements were performed using a Horiba GD-Profiler equipped with a 2 mm Cu anode. The plasma conditions set to obtain a flat crater were 650 Pa Ar pressure and 18 W applied power. The C signal was acquired continuously during the test until the bulk of the material was reached. The samples were cleaned with acetone and then analysed by GDOES. The instrument was calibrated by using a sputtering rate method. For this purpose 20 Certified reference Materials (CRM) and Setting Up Samples (SUS) were used.

Raman spectroscopy (RS, OPTOSKY, ATR 8300 Series, Xiamen, China) measurements were carried out in the spectral range of 200–2000 cm^{-1}, at room temperature and in air by employing a laser wavelength of 785 nm. From preliminary tests the signal in the range below 200 cm^{-1} is background. The spectral resolution was about ±2 cm^{-1}. The laser was focused on the sample by means of a 20 x objective with 0.4 numerical aperture. The Airy diameter is ~3 µm, the beam intensity 450 mW and the acquisition time 20 s.

Surface morphology of the samples has been also investigated by Atomic Force Microscopy (FlexAFM, Nanosurf Liestal, Switzerland) in dynamic force mode.

XPS analyses were performed by using an Escalab 250 Xi spectrometer (Thermo Fisher Scientific Ltd., East Grinstead, UK) with a monochromatic Al X-ray source ($h\nu = 1486.6$ eV) at a spot size of 900 µm. The spectrometer was equipped with a hemispherical analyser and 6-channeltron detection system. The steel samples were investigated in ultra-high vacuum (UHV) at the base pressure in the analysis chamber of about 10^{-9} mbar.

Due to the possible presence of some contaminants, before the analysis each sample was cleaned by Ar^+ ion sputtering (2.0 keV energy and beam current of 1.3 µA mm^{-2}) for 30 s. Afterwards, the main photoelectron spectra of all detected elements were acquired at constant pass energy of 50 eV and standard electromagnetic lens mode, corresponding to ~1 mm in diameter of analysed sample area. After this analysis, the Ar^+ EX06 ion gun was turned on to perform the XPS depth profiling at the same energy and beam current as for initial surface cleaning, with the constant sputtering rate of 0.84 nm/s calculated on the sputtering rate of a Ta_2O_5 reference sample. The binding energy BE = 285.0 eV, corresponding to C1s peak of adventitious C, was used for the scale calibration.

X-ray-induced Auger spectra of the C KLL region were acquired at a pass energy of 100 eV in order to increase the signal-to-noise ratio. Afterwards, the C KLL spectra were smoothed and differentiated using the width of 7 data points to determine the D parameter. Spectroscopic data were acquired and processed by Avantage v.5 software, where the smart mode background subtraction was applied for quantitative analysis.

2.4. Tribological tests and analyses of the worn samples

Wear tests have been carried out on different groups of samples using a pin-on-flat (POF) tribometer (CETR-UMT 3) with a stroke length of 5 mm and a stroke frequency of 5 Hz, at room temperature with applied loads (F_Z) of 10 N and 20 N on an alumina sphere (diameter 9.5 mm) and a test duration of 1 h (the sliding distance S is calculated taking into account the stroke length, stroke frequency and test duration). These conditions correspond to a contact pressure ranging from 700 to 880 MPa, while the sliding speed is of 1 mm/s. The selected loads and the counter-material were selected in agreement to other studies done on similar materials [13]. In addition, alumina was used as counter-material because it has good chemical stability, is stiff and hard, and its volume loss during the tests is negligible. The instrument was equipped with a 2-axis load cell for a continuous measure of both the applied load and the frictional force to determine the coefficient of friction (COF). The volume loss (V) was measured by a stylus profilometer to calculate the wear rate (K) according to the formula:

$$K = \frac{V}{S \bullet F_Z} \tag{2}$$

Surface and cross-section of the worn specimens were then examined by FE-SEM according to the characterization procedure described above.

The morphology of samples inside the wear tracks has been also investigated by AFM.

Finally, Raman spectroscopy measurements were carried out to identify possible compounds resulting from the tribological contact.

3. Results

3.1. Analyses of the plasma treated samples

As shown in Table 1, after plasma treatments the surface hardness remarkably increases and in some cases becomes more than double than that of the original material. Most interesting is the comparison with the same material produced by a conventional process such as forging. Owing to the finer microstructure the hardness of 316 L steel manufactured by L-PBF ($HV_1 = 245 \pm 3$) is greater than that of forged steel ($HV_1 = 148 \pm 2$) and such difference increases after plasma treatments. For instance, the treatment with 2.0 % of CH_4 in the gas mixture enhances the average hardness to 534 ± 36 HV_1 (LPB-F) and 217 ± 6 HV_1 (forged). This is clear from the comparison of hardness profiles vs. surface distance measured in the cross-sections of LPB-F and forged steels after the plasma treatment with 2.0 % of CH_4 (Fig. 3). Therefore, plasma assisted low carburizing treatments of additively manufactured steel are quite promising for industrial applications and their optimization depends on a suitable knowledge of the characteristics of the treated surface layer.

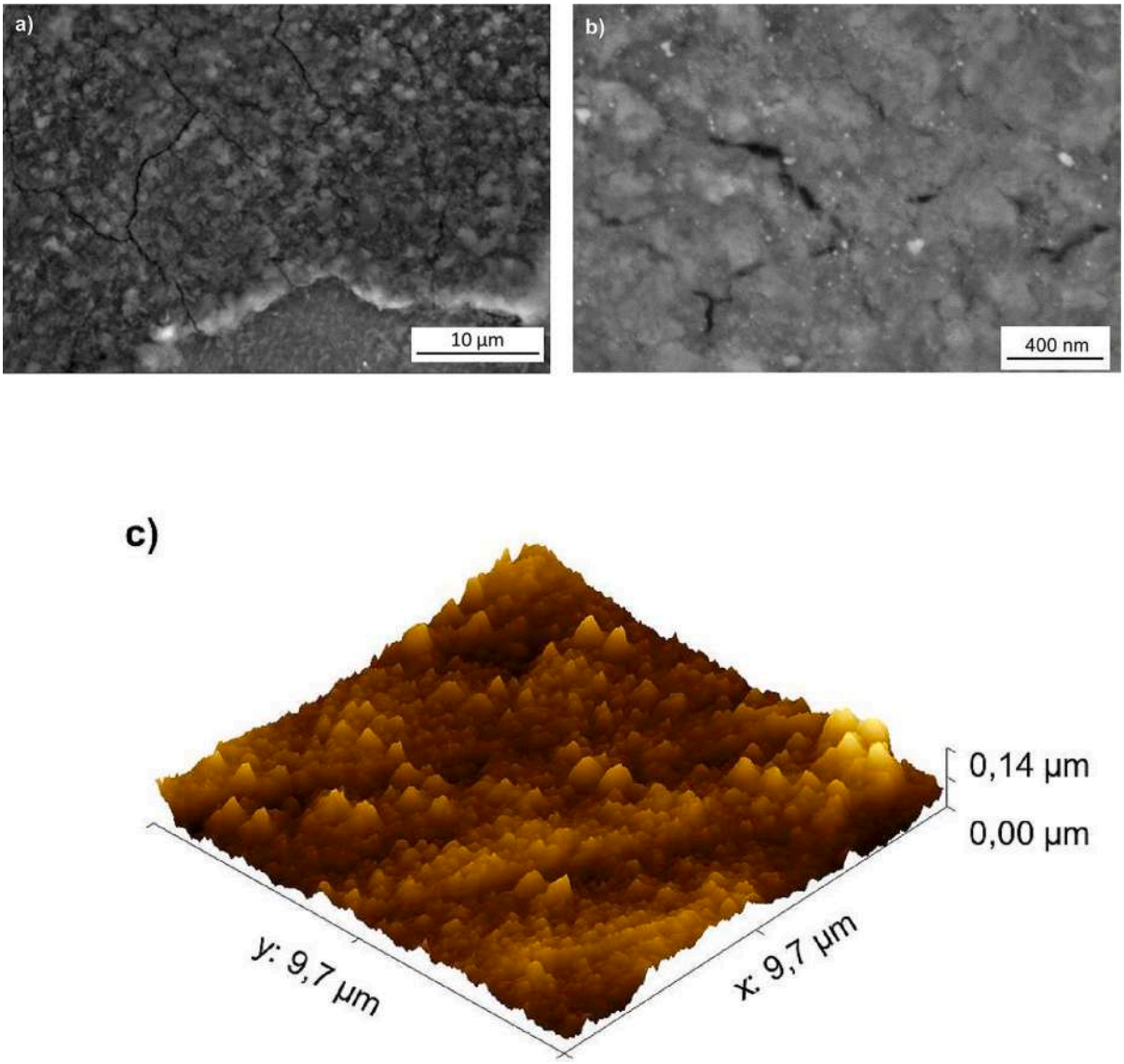

Fig. 5. SEM micrographs in (a) and (b) show the morphology of the C-rich over-layer grown on a sample treated with 2.5 CH_4 + 97.5 H_2. More details are displayed by the AFM image in (c).

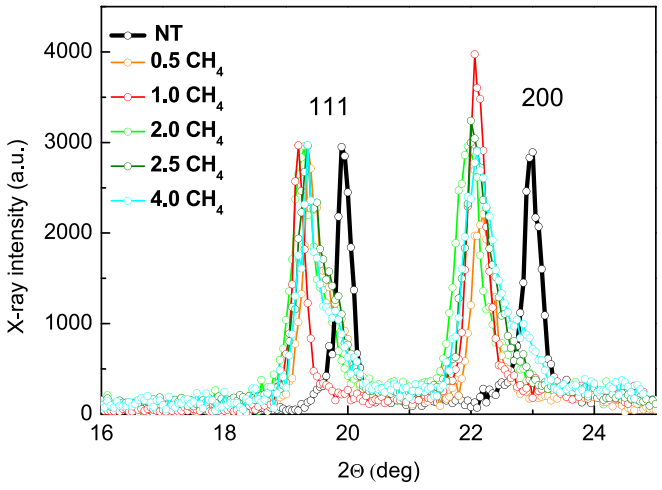

Fig. 6. {111} and {200} XRD peaks of the not treated material (NT) and samples submitted to plasma treatments with different gas mixtures.

The LM micrograph of a cross section (Fig. 4 a) shows the typical S-phase layer that forms on the surface of the samples after plasma treatments. The 25 µm thick layer appears compact and, differently from the austenite below, scarcely affected by etching. At higher magnification, the SEM micrograph in Fig. 4 b) displays a number of slip lines in the S-phase. Moreover, it is observed that a thin over-layer (~2 µm), indicated by red arrows, covers the S-phase. Further details on the morphological features of the over-layer are displayed in the top view of the treated surface (SEM micrograph in Fig. 5 a-b).

The over-layer has been identified as a diamond-like carbon (DLC) by Raman and micro-hardness measurements [34]. It consists of round particles with sub-micrometric size stuck together and presents a network of cracks and detachment zones indicating its intrinsic brittleness. From the topographic AFM image (Fig. 5 c) the surface of the over-layer exhibits a complex morphology made of peaks and valleys with an average peak-valley distance of about 100 nm.

As shown in Fig. 6, the XRD peak positions of all the treated samples result shifted towards lower angles, if compared to those of the untreated steel, highlighting the lattice expansion of S-phase. The lattice parameter a_γ of each group of samples has been determined and the C content calculated by means of Eq. (1). The obtained data are quite

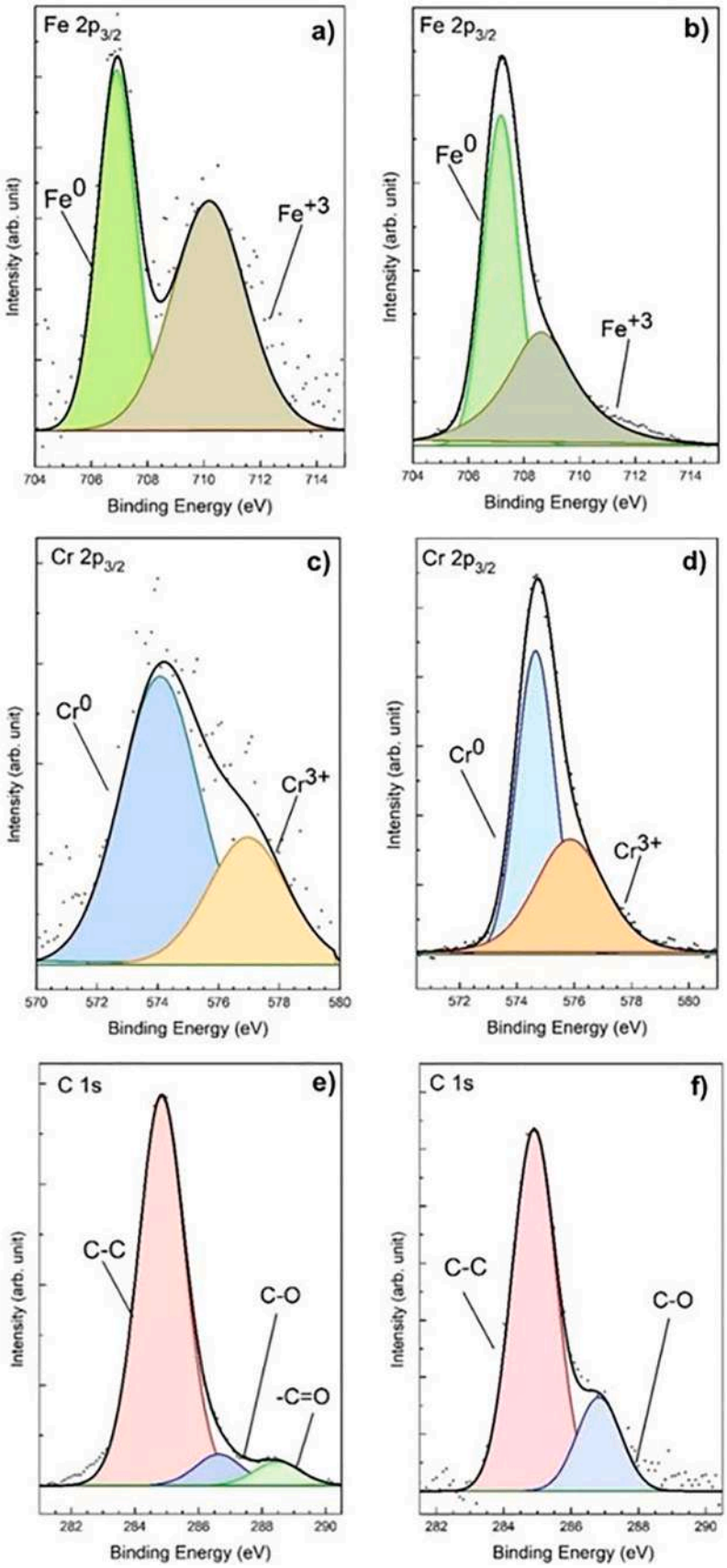

Fig. 7. Peak fitting of Fe $2p_{3/2}$ (a,b), Cr $2p_{3/2}$ (c,d) and C 1 s (e,f) spectra of the samples plasma treated with 2.5 CH_4 + 97.5 H_2, before (a,c,e) and after Ar^+ ion sputtering (b,d,f).

Table 3
Quantitative results of XPS analyses (wt%) of the samples after 30 s of ion sputtering (Ar^+ at 2 keV).

CH_4 (%)	C1	C2	C3	C4	O	Fe^0	Fe^{+3}	Cr^0	Cr^{+3}	Mo^0	Mo^{+3}	Ni^{+2}
BE (eV)	285.0	286.8	288.3	293.2	532.2	707.0	710.0	574.3	576.9	228.1	232.5	853.5
0.5	30.1	10.2	5.7	1.6	31.2	4.7	9.2	1.2	5.3	0.8	–	–
1.0	17.7	–	–	–	34.5	6.1	29.7	1.2	8.4	2.4	–	–
2.0	33.8	2.5	–	–	6.1	20.6	18.0	7.8	7.5	3.7	–	–
2.5	26.4	5.8	–	–	4.6	24.5	18.5	7.5	8.6	4.1	–	–
4.0	14.7	1.4	0.8	–	20.8	12.6	29.5	–	9.6	1.8	–	8.8

similar, around 2.3 wt% C, and the small differences are within the experimental error (± 0.05 wt%). This value, much higher than that of the untreated material, represents the average on a thickness of about 25 μm, which has been estimated by considering the chemical composition of the steel, the absorption coefficients of the elements and the X-ray wavelength used in present experiments [36].

In a previous work [34] Raman spectra have been collected to identify the nature of the over-layer grown on S-phase. C atoms may form a great variety of crystalline and disordered structures because C can exist in sp^3 and sp^2 electronic hybridization states. Between diamond (sp^3) and graphite (sp^2), there are many different DLC phases of amorphous carbon. DLC phases are characterized by a specific ratio of sp^2/sp^3 states [38] and their properties strictly depend on this ratio. The typical diamond peak at 1332 cm^{-1} [39] is not observed in our spectra [34], while the patterns collected from the plasma treated samples exhibit two peaks, namely D-band and G-band peaks. In the pattern of the original untreated material, reported for comparison, they are of negligible intensity, comparable to the background. D and G peaks are due to sp^2 hybridization states and correspond to neighbor atoms moving in opposite directions in the plane of the graphitic sheet (D peak) or perpendicular to this plane (G peak). The D peak is connected to a topological disorder into the graphite layer even if bonding is still sp^2.

XPS measurements have been carried out to analyze the chemical composition of the most external part of the over-layer (few nanometers). To remove the contribution of surface contaminants, the samples were preliminary cleaned by ion sputtering (Ar^+ at 2 keV) for 30 s. For example, Fig. 7 shows the peak fitting of the main XPS spectral components, namely Fe $2p_{3/2}$ (a-b), Cr $2p_{3/2}$ (c-d) and C 1 s (e-f) of a sample treated with a gas mixture containing 2.5 % of CH_4, before (a-c-e) and after Ar^+ ion sputtering (b-d-f).

The C 1 s spectra of every sample were fitted with maximum 4 synthetic peaks: C1 at BE = 285.0 eV (C - C bonds); C2 at BE = 286.8 (C - O bonds); C3 at BE = 288.6 eV (carboxyl groups) and C4 at BE = 293.2 eV (carbonates). The spectra of the steel alloy elements, such as Fe $2p_{3/2}$ and Cr $2p_{3/2}$, were fitted by two synthetic peaks corresponding to metallic and oxidized chemical states: Fe^0 $2p_{3/2}$ at BE = 707.0 eV, Fe^{+3} $2p_{3/2}$ at BE ~710.0 eV; Cr^0 $2p_{3/2}$ at BE = 574.3 eV, Cr^{+3} $2p_{3/2}$ at BE ~576.9 eV. The sputtering eliminates the C components due to carboxyl groups and carbonates, i.e. those due to environmental contamination, whereas in the spectra of Fe 2p and Cr 2p the metallic components are increasing. All the main photoemission peaks are listed in Table 3 together with their BE, weight % and chemical state of the elements.

XPS analyses reveal that C concentration in the all the samples is very high and in some cases larger than 30 %. These values are much higher than those of the S-phase measured by XRD. In addition to C, the presence of O, Fe, Cr and Mo was revealed on the samples surface while the signal of Ni was detected only in the sample prepared with 4 % of CH_4. Furthermore, Fe and Cr were found in the metallic and oxidized states; the low amount of metals registered by XPS indicates that in some points the coverage of C is very thin or presents cracks (see Fig. 5).

From depth profiles, displayed in Fig. 8, C content on the surface steeply decreases within ~200–250 nm but its value remains remarkably high down to 800 nm. This trend of depth profiles can be understood by considering the high surface roughness of the samples. Fe and Cr profiles display the opposite trend while Mo content is nearly constant.

DLC phases are characterized by a specific ratio (sp^2/sp^3) of C states, but the electronic configuration can not be determined from the analysis of C 1 s spectra [40]. However, it can be identified from the value of D parameter, determined from Auger C KLL spectrum. The D parameter is defined as the difference of kinetic energy between the maximum and the absolute minimum in the first derivative of C KLL spectrum [41]. For the graphite with planar structure, the D parameter has the value of 21.2 eV, whereas D = 13.7 eV for diamond with tetrahedral structure. The specific sp^2/sp^3 C hybridization ratio can be determined from intermediate values of D parameter. The precision of D parameter depends on the quality of Auger C KLL spectrum, i.e., in the case of noisy spectra, the smoothing and differentiation procedures can give an error up to about 0.5 eV. C 1 s spectra of the examined samples are shown in Fig. 9 (a), whereas the first derivatives of Auger C KLL spectra are plotted in Fig. 9 (b).

The values of D parameter, determined for all the samples after 30 s cleaning by Ar^+ ion sputtering, are reported in Table 4. D parameter always indicates a prevalence of sp^3 bonds, that reaches 100 % in the samples treated with a content of CH_4 in gas mixture ≥2.0 %.

The D parameter was determined after 30 s cleaning by Ar^+ ion sputtering, however it was not possible to measure its depth profile because a longer time of ion bombardment can modify the C electronic configuration.

C content vs. surface distance has been measured through Rf-GDOES in the layers affected by plasma treatments. Typical C profiles are displayed in Fig. 10: the initial high values correspond to the over-layer, then C signals show typical diffusive profiles in the S-phase with some differences depending on the treatment. The trends are in good agreement with those of micro-hardness measured in the cross-sections of the samples [34] indicating that the hardness of S-phase mainly depends on the C amount.

3.2. Tribological tests and analyses of the worn samples

Fig. 11 shows the wear rate results of samples prepared with different plasma treatments after tribological tests carried out with loads of 10 N and 20 N. Data show how all the plasma treatments lead to a remarkable improvement of wear resistance with respect the untreated material. This demonstrates the effectiveness of the low-temperature carburizing process assisted by plasma on the tribological behavior of AM 316 L steel. For both the applied loads the wear rate K increases with CH_4 content in the gas mixture.

COF plots vs. time recorded in tests at 10 and 20 N are shown in Fig. 12 (a-b). At the beginning of the test COF values of all the treated samples are low (~ 0.2), then they increase and become substantially stable, even if the signals are quite noisy and exhibit several oscillations. In some cases signal oscillations are present also in running-in regime. The initial relevant variation is not observed in the untreated material.

As displayed by Fig. 12 (c), in the tribological tests at 20 N COF exhibits a slight decreasing trend as CH_4 content in the gas mixture increases and above 1 % its value becomes lower than that of the untreated steel. The samples tested at 10 N show some variations depending on CH_4 content, however their values are always greater than that of the untreated material.

To understand the results of tribological tests the sample surface inside the wear tracks has been investigated through different experimental techniques.

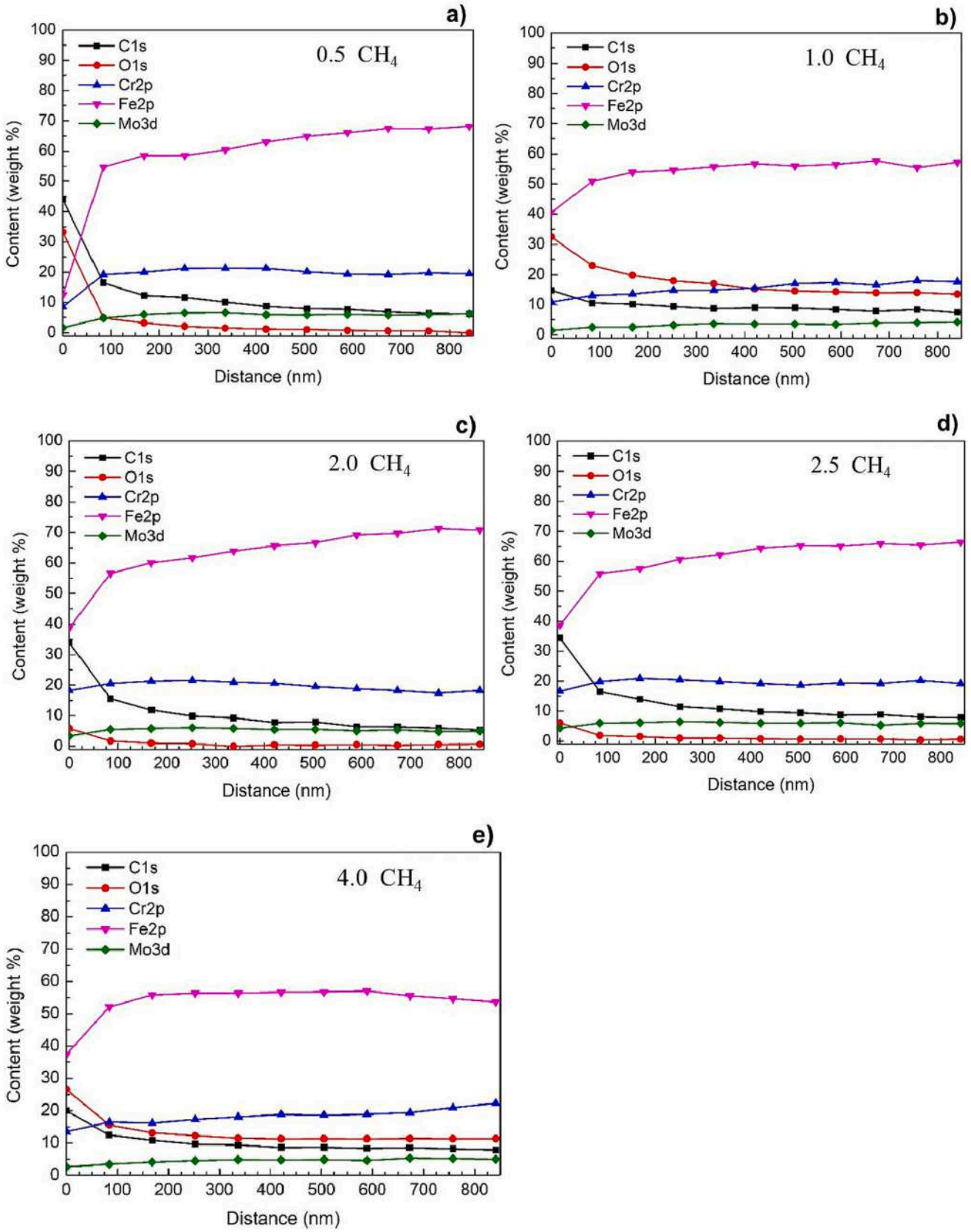

Fig. 8. XPS depth profiles of the samples submitted to plasma treatments.

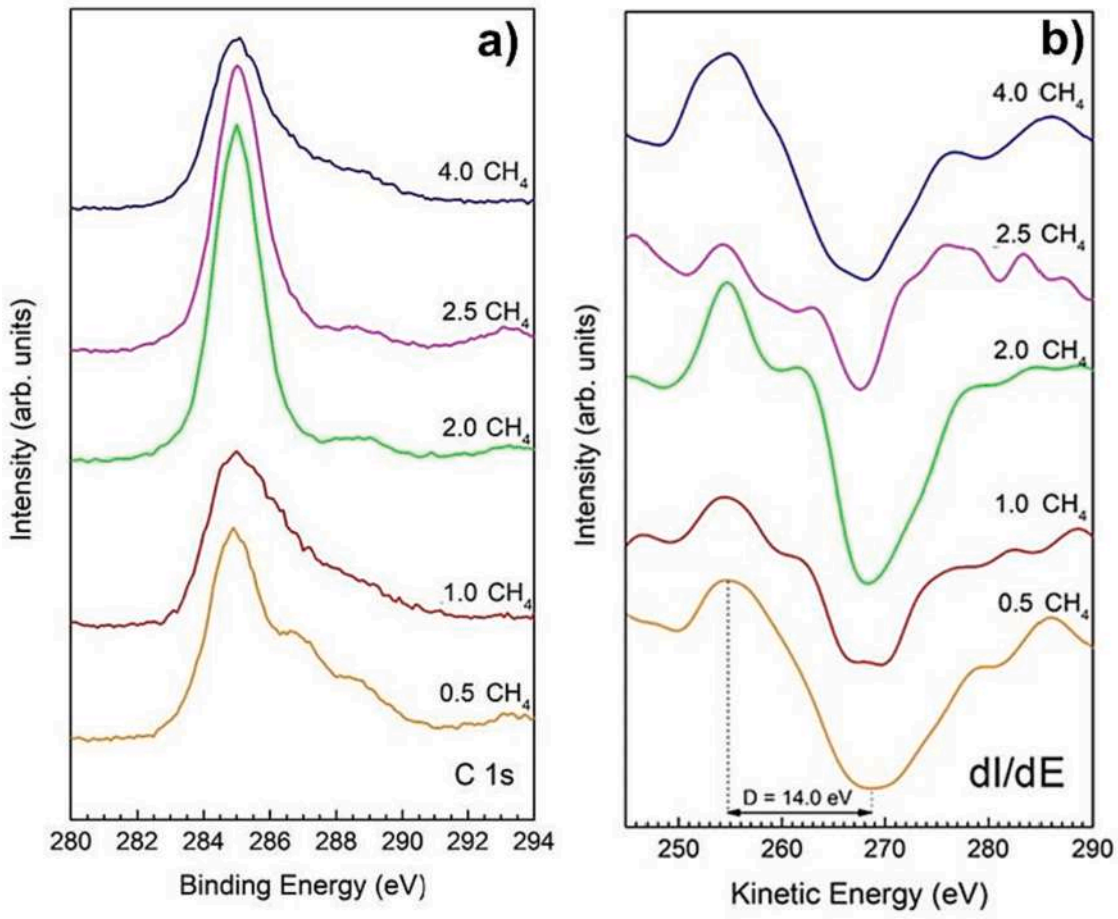

Fig. 9. Comparison between C 1 s spectra (a) and first derivatives of the C KLL spectra (b) for all the samples. The D parameter is the difference of kinetic energy between the maximum and the absolute minimum in the first derivative of C KLL spectrum.

Table 4
D parameter determined from the derivative of C KLL spectra of plasma treated 316 L samples and corresponding percentage of sp^3 bonds.

CH_4 content	0.5 %	1.0 %	2.0 %	2.5 %	4.0 %
D parameter (eV)	14.0	15.0	13.7	12.7	13.5
sp^3 bonds (%)	96	83	100	100	100

Triboxidation combined with abrasive wear was demonstrated by SEM analysis of the wear marks (Fig. 13). The micrographs also show an increase of abrasive scars as CH_4 content in the gas mixture increases. Moreover, wear tracks are covered not only by triboxides (dark gray areas) but also by C-rich deposits (black areas), the amount of which increases with CH_4. Triboxidation increases also with greater applied load.

At the end of the tests, the cross-section analysis of the tribological layer shows that part of the S-phase has been removed, however the unaffected austenite below it has been never exposed to the tribocontact (Fig. 14 a). For all the plasma treated samples the wear traces are within the thickness of the S-phase layer. The graph in Fig. 14 (b) shows the ratio between the maximum wear track depth and S-phase thickness for samples treated in different conditions. In agreement with the results reported in Fig. 11, it is observed that penetration depth increases with CH_4 content in the gas mixture, but the ratio never exceeds 85 %, i.e. the wear trace is always within the S-phase.

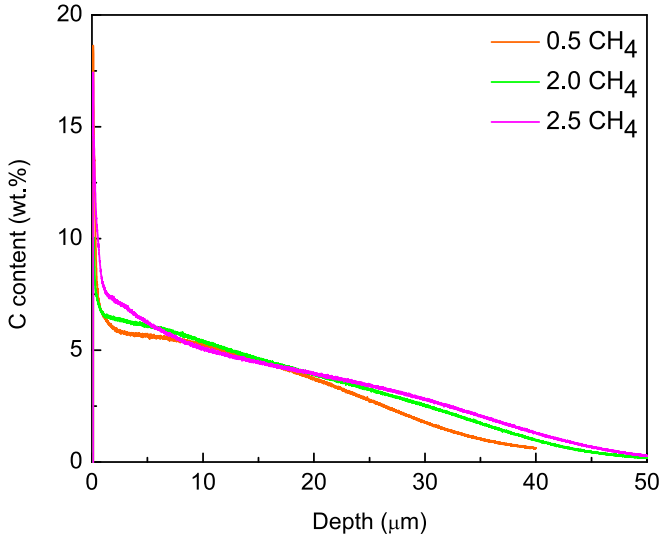

Fig. 10. C content vs. surface distance measured through GDOES in the layers affected by plasma treatments.

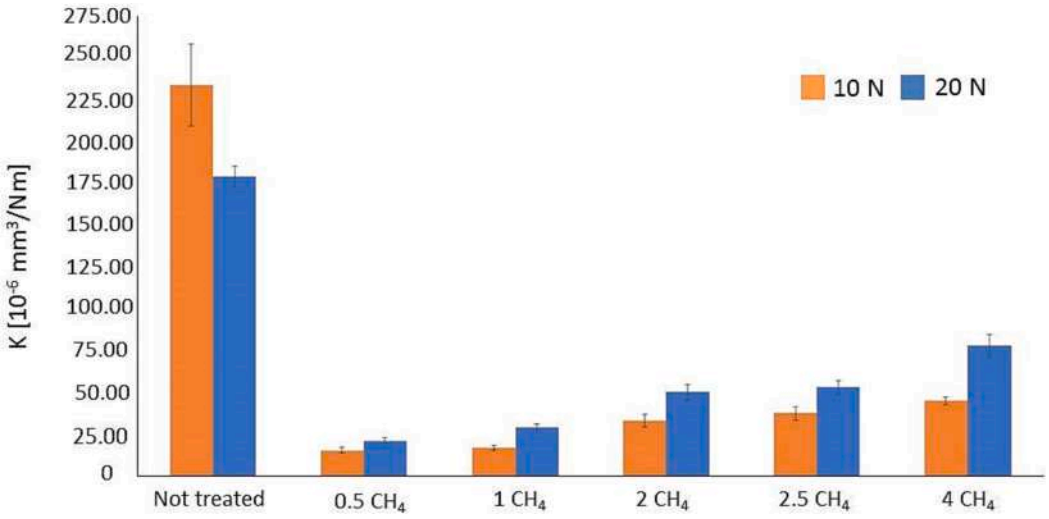

Fig. 11. Wear rate K of samples submitted to plasma treatments with different gas mixtures. Results of tribological tests performed at 10 N and 20 N.

AFM micrographs taken inside the wear tracks show a scenario of valleys and peaks; roughness on nanometric scale increases with applied load and CH_4 content in the gas mixture. An example is reported in Fig. 15 that compares the surface morphology of samples plasma treated with 0.5 and 4.0 % of CH_4 and submitted to tribological tests at 10 N and 20 N.

Raman spectra in Fig. 16 were collected on the wear tracks, more specifically (a) and (b) on C-rich deposits while (c) and (d) on tribo-oxides. The absence of D and G peaks in samples tested at both 10 N (a) and 20 N (b) indicates that the DLC over-layer has been completely removed. In fact, the C-rich deposits are not enough thick to give rise to significant Raman peaks. Preliminary tests evidenced that the signal in the range below 200 cm^{-1} is background thus this part of the spectrum is not reported here. No peaks were detected in the range 700–1000 cm^{-1} while in the part of the spectrum at lower Raman number, 200–700 cm^{-1} (c-d), some peaks have been observed and identified as those of hematite α-Fe_2O_3, lepidocrocite γ-FeO(OH) and goethite α-FeO(OH) [42]. Slight differences of peak positions with respect the values reported in ref. [42] can be explained by considering that, in this case, also Cr contributes to form these compounds (mixed Fe—Cr oxides and hydroxides). The same material submitted to tribological tests in as-built condition was previously investigated by Lanzutti et al. [43] who observed intense peaks at 220, 280, 390, 495, 612 and 690 cm^{-1}, which were attributed to a spinel of Fe and Cr oxide, $Fe_{(1+X)}Cr_{(1-X)}O_3$. Raman spectra displayed in Fig. 16 (c-d) exhibit very weak signals in these positions indicating that the DLC over-layer probably limits the ability of the steel surface to form a thick oxide layer.

4. Discussion

On the basis of the results from XRD, Raman and XPS, three techniques with different depth of analysis, the surfaces of the samples after plasma treatments exhibit a complex scenario. A layer of expanded austenite (S-phase) with a thickness of ~25 μm is formed on the samples surface. S-phase is covered by a 2-μm thick over-layer, much richer of C, that is not homogeneous: XPS depth profiles show a decreasing trend of C concentration as surface distance increases. Moreover, the inner part of the over-layer consists of amorphous C (sp^2 bonds) with a certain degree of topological disorder, whereas in the outer one C exhibits both sp^2 and sp^3 hybridization states with a high prevalence of sp^3 ones. It was not possible to measure the specific trend of C hybridization ratio (sp^2/sp^3) vs. the distance from the surface, because ion bombardment during XPS depth profiling modifies its electronic configuration, however Raman spectroscopy, whose depth of analysis is few tens of nanometers [44], indicates only the presence of sp^2 bonds. Therefore, it is reasonable to suppose that sp^3 states steeply decrease going to zero at a distance from the surface of about 10–15 nm.

Another relevant issue is that the over-layer is much harder than the S-phase. In a previous work [34] Vickers micro-hardness tests, performed on the plasma exposed surfaces by applying different loads from 25 to 1000 g (different amounts of over-layer and S-phase are involved in each test [45–47]), showed that hardness is very high up to a penetration depth of ~2 μm (over-layer thickness) with values consistent with DLC [48].

To explain the presence of the C-rich over-layer and its structure it is useful to consider that gas mixtures consisting of H_2 and CH_4 are commonly used to grow synthetic polycrystalline diamond films on metallic substrates. Since the most stable C phase is graphite and the activation energy for graphite-diamond transition is very high (~ 0.4 eV/atom), the nucleation and growth of meta-stable diamond crystals on non-diamond substrates under CVD conditions have been extensively discussed in literature (e.g. see refs. [49–51]). A model for diamond nucleation by energetic species, proposed by Lifshitz et al. [52], involves spontaneous bulk nucleation of diamond embryos in an amorphous C hydrogenated matrix and ion bombardment-induced growth through a preferential displacement mechanism. Recently, this model has been confirmed by TEM observations of Li et al. [53].

On these grounds, we believe that the transformation of the material due to plasma treatments can be a two-stage process. In the first stage C atoms enter the metal and expand austenite forming the S-phase. XRD results show that the C content in all the examined samples is about 2.3 wt% which represents an upper limit of oversaturation. The presence of several slip lines in the S-phase (Fig. 4 b) indicates that part of the elastic strains due to the oversaturation of austenite is released in form of plastic deformation. In the second stage, since the lattice of austenite is not able to allocate further C atoms they deposit on the surface forming the over-layer. Its thickness and characteristics depend on the specific gas mixture used in the plasma treatment, anyway this DLC layer is brittle and much harder than S-phase. It is well known from literature that huge residual stresses accumulate within DLC coatings on steel and

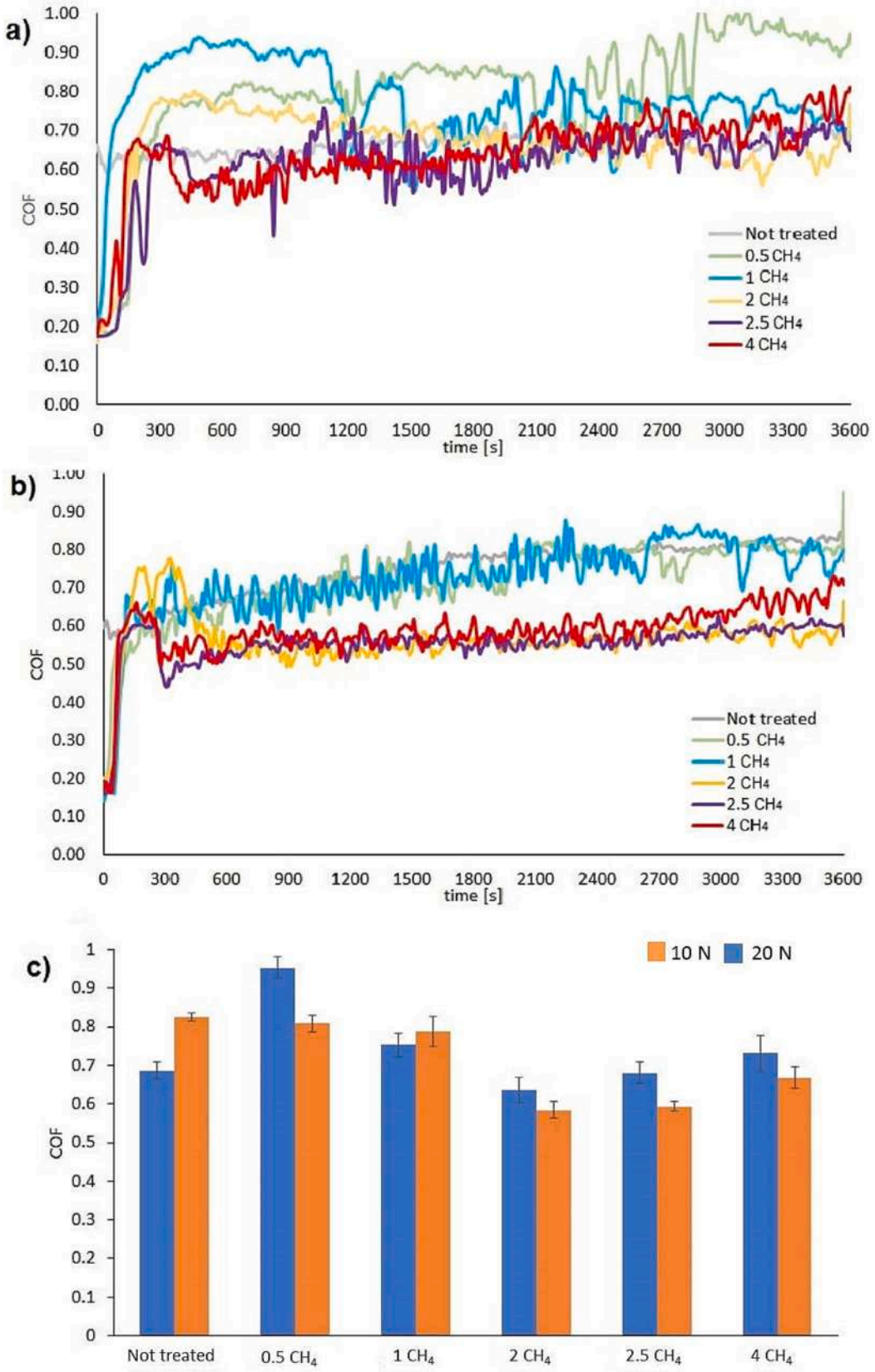

Fig. 12. COF vs. sliding time in tribological tests performed at 10 N (a), 20 N (b) and average COF at the end of the test (c).

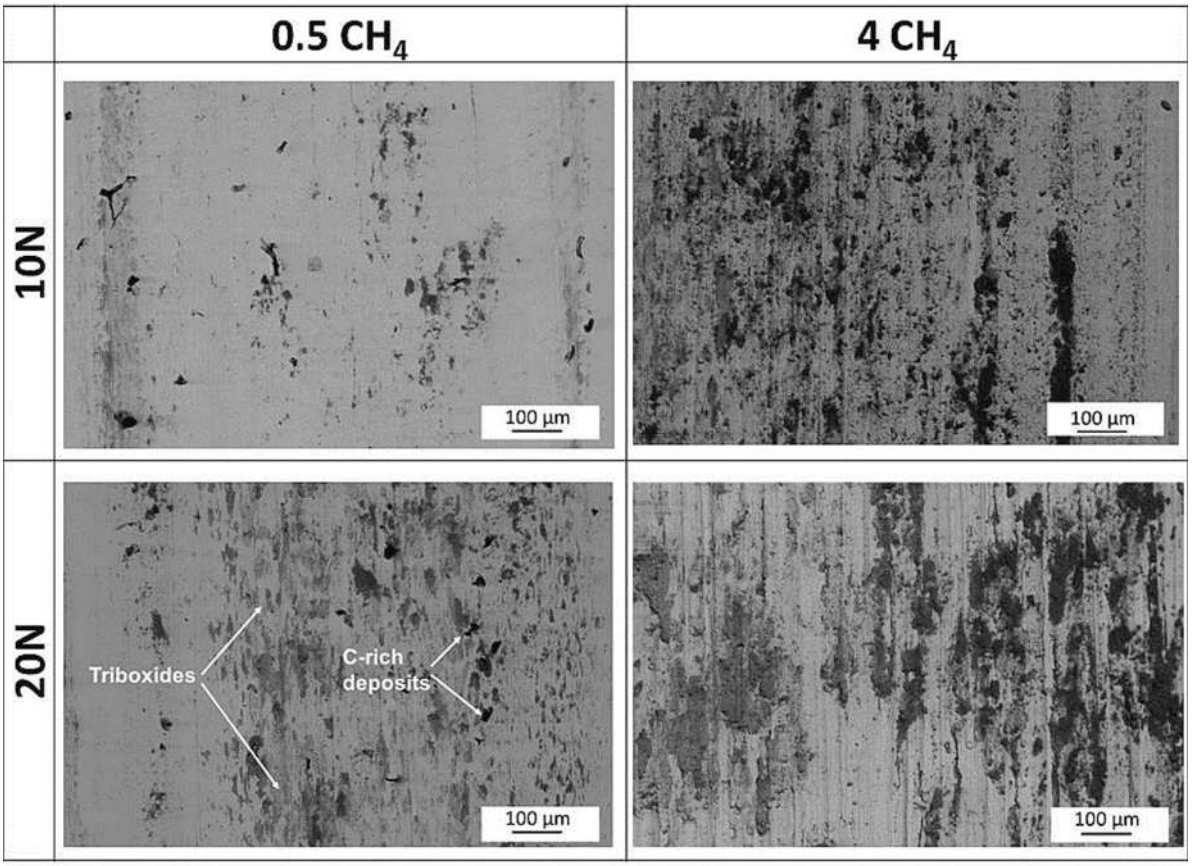

Fig. 13. Representative SEM micrographs of the wear track in the samples plasma treated with 0.5 % and 4 % of CH_4 in the gas mixture; tested at 10 N and 20 N. Tracks are partially covered by triboxides (dark gray areas) and C-rich deposits (black areas).

cause coating cracking and delamination [53]. They originate from lattice mismatch and thermal strain between coating and substrate thus an interlayer (e.g. CrN, WC, TiAlN, TiC, TiCN, ZrN or ZrC) is usually deposited on steel surface to avoid coating detachment [54–56].

As shown in Fig. 11, independently on the gas mixture used in the treatment, plasma assisted low temperature carburizing leads to a remarkable increase of the wear resistance of 316 L steel produced by AM. This behavior is consistent with the results of micro-hardness tests presented elsewhere [34]. In fact, the low temperature carburizing process produces an increase in the surface hardness of the material: on the top surface for the production of the thin/hard layer and of the S-phase layer in the substrate. It should be noted that the top surface layer is also brittle and acts as an anti-wear barrier for a very short time during the test. Since wear tracks (see Fig. 14) affect only the S-phase and not the austenite below thus the improved tribological performance is due to the greater hardness of expanded austenite.

The slight differences between the samples treated with increasing amounts of CH_4 in the gas mixture can be explained by considering the role played by DLC over-layer. At the beginning of the tribological tests the solid-lubricating performance of DLC leads to low COF values (~ 0.2) which then increase because the over-layer fractures owing to its intrinsic brittleness and detaches from the metallic substrate. Even if in some samples few oscillations are also observed during running-in regime, in general COF signals increase continuously without abrupt changes. This indicate that there is a gradual detachment of DLC over-layer. Moreover, the underneath material (expanded austenite) strongly contributes to bear the applied load. The COF transition from 0.2 to the plateau value corresponds to the passage from a surface covered by DLC to its complete detachment. Likely, the gradual loss of the over-layer leads to alternated surface areas with and without DLC

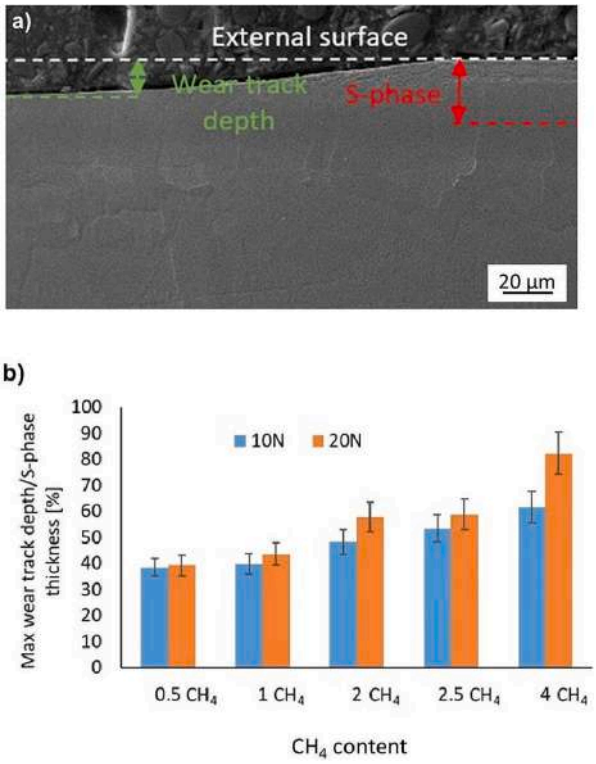

Fig. 14. Graph showing the relationship between the relative wear trace depth with respect to the S phase thickness as a function of the methane content for the samples tested at both 10 N and 20 N.

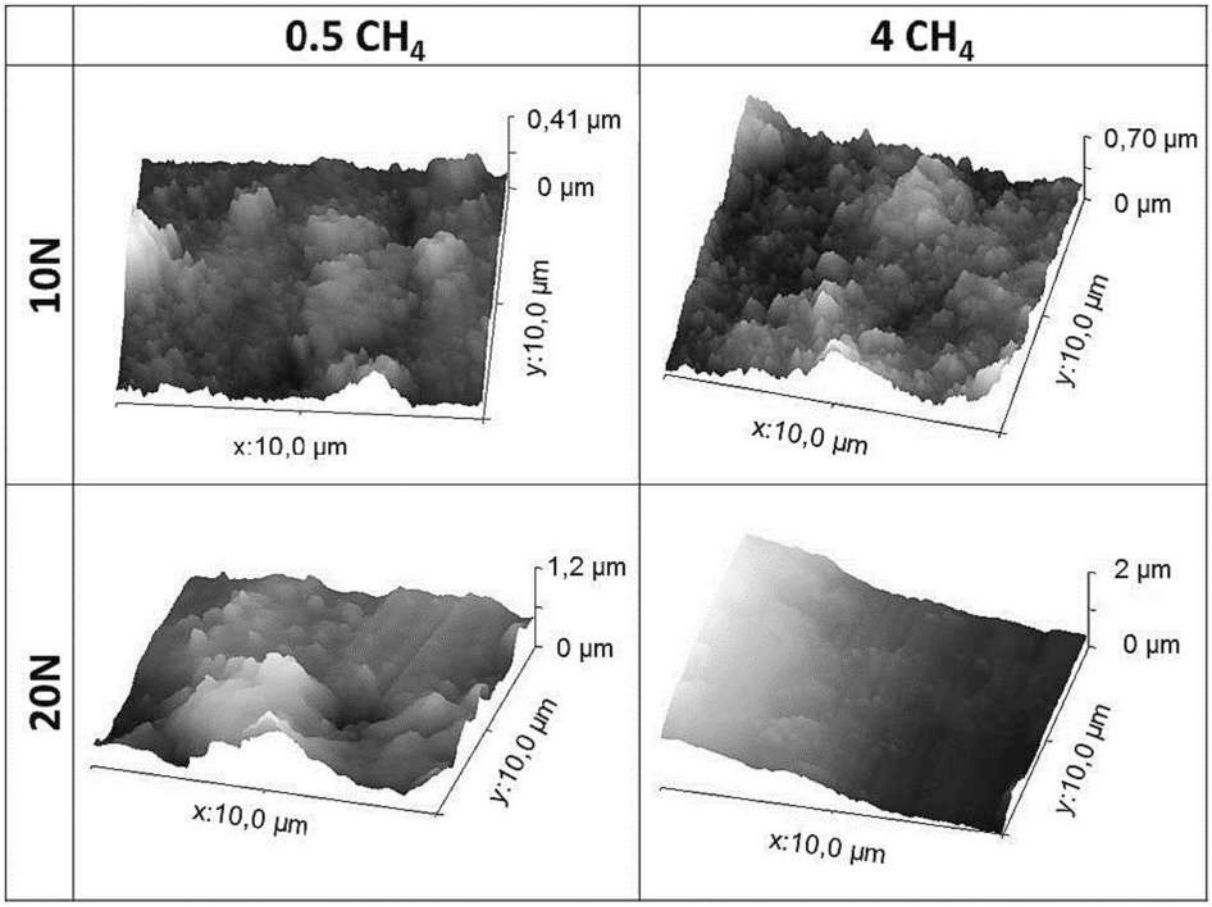

Fig. 15. AFM images taken in the central area of wear tracks of the samples treated with 0.5 and 4 % of CH_4 in the gas mixture; tested at both 10 N and 20 N.

cover. The destruction of DLC over-layer produces DLC debris acting as abrasive particles, i.e. they behave as a third body during tribocontact, and the wear mechanism changes to abrasion.

Since sp. bonds in the DLC near the surface are completely sp^3 if CH_4 is above 1 % (see Table 4), the particle hardness increases with CH_4 content and consequently the wear rate. This effect of sp^3 bonds has been clearly observed in the samples tested with both applied loads. The presence of abrasive wear is also evidenced by COF signals, which are very noisy in all the treated samples when compared to that of the untreated material.

Moreover, when a significant amount of DLC is transferred on the tracks during the tests a slightly reduction of COF is observed (Fig. 10 c) and such effect is likely related to the inner part of the over-layer, richer of amorphous C (sp^2 bonds). Once the DLC over-layer is broken, part of fragmented amorphous C is transferred on the tracks (see Fig. 13) forming a barrier layer between counter material and steel; the phenomenon is more evident at higher applied loads, due to more efficient fragmentation of the over-layer, and with higher CH_4 content in the gas mixture. This effect of DLC on stainless steels has also been studied under water lubrication conditions [57].

On the basis of these considerations we believe that the optimal tribological behavior could be achieved if plasma treatments produce the S-phase layer but not the DLC over-layer.

5. Conclusions

316 L steel samples, manufactured by L-PBF and submitted to low temperature carburizing treatments assisted by plasma with different gas mixtures, have been submitted to tribological tests at 10 N and 20 N. They have been examined before and after the tests and the results can be summarized as follows.

1. Microstructural and chemical analyses of the surface before tribological tests show that all the treatments give rise to a surface layer of expanded austenite (S-phase) with thickness of ~25 µm covered by a 2 µm thick DLC over-layer that is brittle and much harder than S-phase.
2. In the outer part of DLC there is a prevalence of sp^3 bonds, that reaches 100 % in the samples treated with a content of CH_4 in the gas mixture ≥2.0 %.
3. Independently on the gas mixture used in plasma treatment, all the samples exhibit a wear resistance much better than that of the untreated material.
4. Wear resistance of the samples also depends on plasma treatment conditions: the greater the CH_4 content, the lower the wear resistance. Owing to its intrinsic brittleness the DLC over-layer fractures and detaches from the metal surface during the tests and the hard debris take part to the wear process acting as abrasive particles which contribute to increase the wear rate.

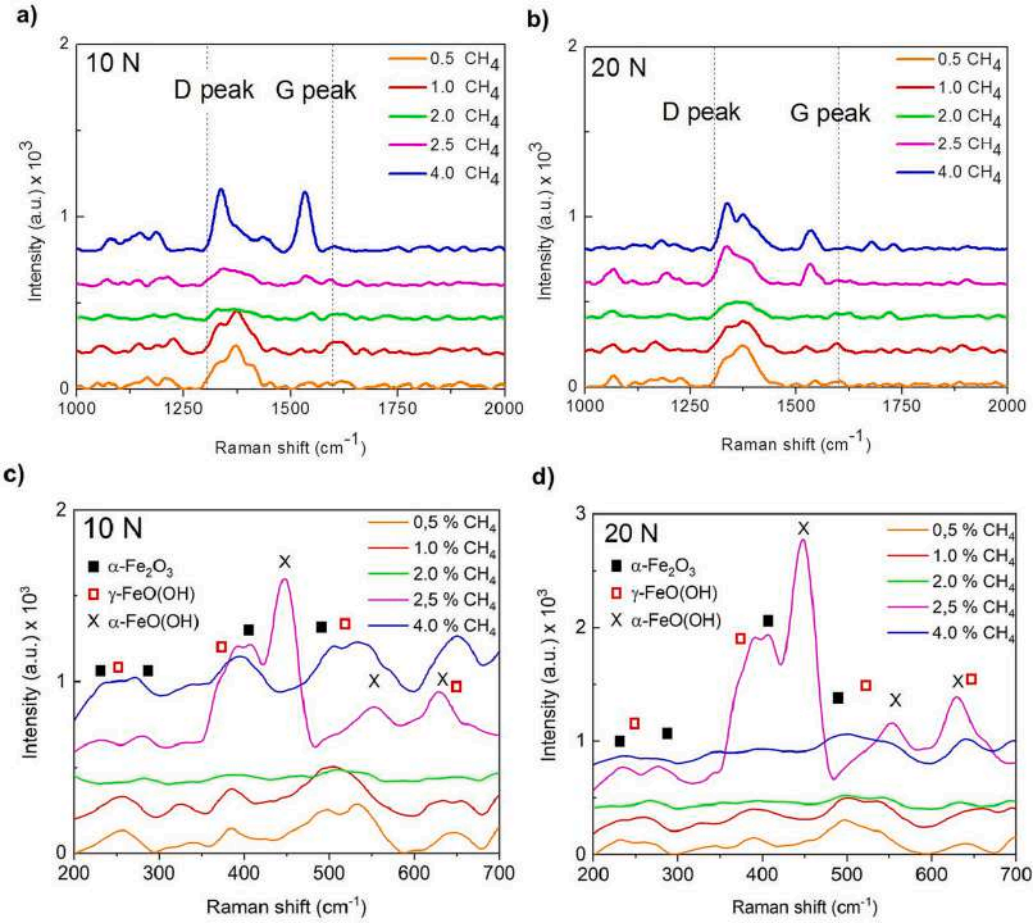

Fig. 16. Two sections of Raman spectra of the samples submitted to plasma treatments with different gas mixtures after tribological tests at 10 N (a-c) and 20 N (b-d). Spectra in (a) and (b) were collected on C-rich deposit (black areas in Fig. 13). Dashed lines in (a) and (b) indicate the positions of D and G peaks. The symbols in (c) and (d) indicate the positions of hematite α-Fe_2O_3, lepidocrocite γ-FeO(OH) and goethite α-FeO(OH) according to ref. [42]. Spectra in (c) and (d) were collected on tribo-oxides (dark gray areas in Fig. 13).

5. During the tests the transfer of some DLC on the metal surface tends to slightly decrease COF, however without significant effects on wear resistance.

It can be concluded that the optimal tribological behavior can be achieved if plasma treatments produce the S-phase layer but not the DLC over-layer. Therefore, future research will be oriented to find the suitable combination of treatment time and gas composition to reach this scope.

CRediT authorship contribution statement

E. Bolli: Investigation. **S. Kaciulis:** Formal analysis. **A. Lanzutti:** Conceptualization, Writing – original draft, Writing – review & editing. **A. Mezzi:** Formal analysis. **R. Montanari:** Supervision, Writing – original draft, Writing – review & editing. **A. Palombi:** Investigation. **F. Sordetti:** Investigation. **E. Vaglio:** Investigation, Methodology. **A. Varone:** Conceptualization, Writing – original draft, Writing – review & editing. **C. Verona:** Formal analysis, Investigation.

Declaration of competing interest

The authors declare that they have no known competing financial interests or personal relationships that could have appeared to influence the work reported in this paper.

Data availability

Data will be made available on request.

Acknowledgments

The authors are grateful to Mr. Piero Plini and Dr. Emanuela Sgreccia of Department of Industrial Engineering – University of Rome "Tor Vergata" for the assistance in sample preparation and Raman measurements. The Laboratory for Advanced Mechatronics – LAMA FVG – of the University of Udine is also gratefully acknowledged, in particular Prof. M. Sortino and Prof. G. Totis. LAMA FVG is an international research centre for product and process innovation where the three Universities of Friuli Venezia Giulia Region (Italy) synergically cooperate for promoting Research and Development activities at academic and industrial level.

Emanuele Vaglio is grateful for funding under the REACT EU Italian PON 2014-2020 Program - Action IV.4 - Innovation (DM 1062, 10/08/2021).

References

[1] J.R. Davis, Surface engineering of stainless steels, in: C.M. Cotell, J.A. Sprague, F. A. Smidt Jr. (Eds.), ASM Handbook Volume 5, Surface Engineering, ASM International, 1994, pp. 741–761, https://doi.org/10.31399/asm.hb.v05.a0001305.

[2] K.L. Hsu, T.M. Ahn, D.A. Rigney, Friction, wear and microstructure of unlubricated austenitic stainless steels, Wear 60 (1980) 13–37, https://doi.org/10.1016/0043-1648(80)90247-1.

[3] S.R. Collins, P.C. Williams, S.V. Marx, A.H. Heuer, F. Ernst, H. Kahn, Low-temperature carburization of austenitic stainless steels, in: J. Dossett, G.E. Totten (Eds.), ASM Handbook, Volume 4D, Heat Treating of Irons and Steels, ASM International, 2014, pp. 451–460.

[4] S.K. Balijepalli, I. Colantoni, R. Donnini, S. Kaciulis, M. Lucci, R. Montanari, N. Ucciardello, A. Varone, Modulo elastico della fase S in un acciaio 316 L kolsterizzato, Metall. Ital. 1 (2013) 42–47.

[5] S.K. Balijepalli, R. Donnini, S. Kaciulis, R. Montanari, A. Varone, Young's modulus profile in kolsterized AISI 316 L steel, Mater. Sci. Forum 762 (2013) 183–188.

[6] G.M. Michal, F. Ernst, H. Kahn, Y. Cao, F. Oba, N. Agarwal, A.H. Heuer, Carbon supersaturation due to paraequilibrium carburisation: stainless steels with greatly improved mechanical properties, Acta Mater. 54 (2006) 1597–1606, https://doi.org/10.1016/j.actamat.2005.11.029.

[7] J. Gentil, F. Ernst, G. Michal, A.H. Heuer, (2006) The effect of colossal carbon supersaturation on stainless steels of the type PH13-8Mo and AL6XN, MS&T 2006, in: Proceedings from the Materials Science & Technology Conference., Cincinnati, OH, 15–19 October 2006.

[8] L. Ceschini, C. Chiavari, E. Lanzoni, C. Martini, Low-temperature carburised AISI 316 L austenitic stainless steel: wear and corrosion behavior, Mater. Des. 38 (2012) 154–160, https://doi.org/10.1016/J.MATDES.2012.02.019.

[9] Y. Sun, L.Y. Chin, Residual stress evolution and relaxation in carbon S phase layers on AISI 316 austenitic stainless steel, Surf. Eng. 18 (2002) 443–446, https://doi.org/10.1179/026708402225010029.

[10] N. Agarwal, H. Kahn, A. Avishai, A.H. Heuer, G. Michal, F. Ernst, Enhanced fatigue resistance in 316L austenitic stainless steel due to low-temperature paraequilibrium carburization, Acta Mater. 55 (2007) 5572–5580, https://doi.org/10.1016/j.actamat.2007.06.025.

[11] Y. Jiang, Y. Li, Y. Peng, J. Gong, Mechanical properties and cracking behavior of low-temperature gaseous carburized austenitic stainless steel, Surf. Coat. Technol. 403 (2020) 126343, https://doi.org/10.1016/j.surfcoat.2020.126343.

[12] J. Qu, P.J. Blau, B.C. Jolly, Tribological properties of stainless steels treated by colossal carbon supersaturation, Wear 263 (2007) 719–726, https://doi.org/10.1016/j.wear.2006.12.049.

[13] Y. Sun, T. Bell, Dry sliding wear resistance of low temperature plasma carburised austenitic stainless steel, Wear 253 (2002) 689–693.

[14] Y. Sun, Tribocorrosion behavior of low temperature plasma carburized stainless steel, Surf. Coat. Technol. 228 (2013) S342–S348, https://doi.org/10.1016/j.surfcoat.2012.05.105.

[15] Y. Sun, R. Bailey, Comparison of Wear performance of low temperature Nitrided and carburized 316L stainless steel under dry sliding and corrosive-Wear conditions, J. Mater. Eng. Perform. 32 (2023) 1238–1247, https://doi.org/10.1007/s11665-022-07182-9.

[16] F. Rotundo, L. Ceschini, C. Martini, R. Montanari, A. Varone, High temperature tribological behaviour and microstructural modifications of the low-temperature carburised AISI 316 L austenitic stainless steel, Surf. Coat. Technol. 258 (2014) 772–781, https://doi.org/10.1016/j.surfcoat.2014.07.081.

[17] Y. Sun, X. Li, T. Bell, Low temperature plasma carburising of austenitic stainless steels for improved wear and corrosion resistance, Surf. Eng. 15 (1) (1999) 49–54, https://doi.org/10.1179/026708499322911647.

[18] Y. Sun, Kinetics of low temperature plasma carburizing of austenitic stainless steels, J. Mater. Process. Technol. 168 (2) (2005) 189–194, https://doi.org/10.1016/j.jmatprotec.2004.10.005.

[19] I. Ciancaglioni, R. Donnini, S. Kaciulis, A. Mezzi, R. Montanari, N. Ucciardello, G. Verona Rinati, Surface modification of austenitic steels by low temperature carburization, Surf. Interface Anal. 44 (2012) 1001–1004, https://doi.org/10.1002/sia.4894.

[20] S.K. Balijepalli, L. Ceschini, I. Ciancaglioni, S. Kaciulis, A. Mezzi, R. Montanari, C. Martini, G. Verona Rinati, Corrosion effect to the surface of stainless steel treated by two processes of low temperature carburization, Surf. Interface Anal. 46 (2014) 731–734, https://doi.org/10.1002/sia.5456.

[21] S.J. Gobbi, V.J. Gobbi, G. Reinke, Improvement of mechanical properties and corrosion resistance of 316L and 304 stainless steel by low temperature plasma cementation, Matéria (Rio J.) 25 (2020), https://doi.org/10.1590/s1517-707620200002.1036 e-12636.

[22] H.Y. Liu, H.L. Che, G.B. Li, M.K. Lei, Low-pressure hollow cathode plasma source carburizing technique at low temperature, Surf. Coat. Technol. 422 (2021) 127511, https://doi.org/10.1016/j.surfcoat.2021.127511.

[23] H.Y. Liu, H.L. Che, J.Y. Gao, G.B. Li, M.K. Lei, Low-pressure hollow cathode plasma source carburizing of AISI 304L austenitic stainless steel at low temperature, Surf. Coat. Technol. 442 (2022) 128548, https://doi.org/10.1016/j.surfcoat.2022.128548.

[24] R.A. Savrai, P.A. Skorynina, A.V. Makarov, A.I. Men'shakov, V.S. Gaviko, The influence of frictional treatment and low-temperature plasma carburizing on the structure and phase composition of metastable austenitic steel, Phys. Met. Metallogr. 124 (2023) 496–503, https://doi.org/10.1134/S0031918X23600483.

[25] T. Kurzynowski, K. Gruber, W. Stopyra, B. Kuznicka, E. Chlebus, Correlation between process parameters, microstructure and properties of 316 L stainless steel processed by selective laser melting, Mater. Sci. Eng. A 718 (2018) 64–73, https://doi.org/10.1016/j.msea.2018.01.103.

[26] J.N. Lemke, R. Casati, N.F.M. Lecis, C. Andrianopoli, A. Varone, R. Montanari, M. Vedani, Design of wear-resistant austenitic steels for selective laser melting, Metall. Mater. Trans. A 49 (2018) 962–971, https://doi.org/10.1007/s11661-017-4461-7.

[27] Y.M. Wang, T. Voisin, J.T. McKeown, J. Ye, N.P. Calta, Z. Li, Z. Zeng, Y. Zhang, W. Chen, T.T. Roehling, R.T. Ott, M.K. Santala, P.J. Depond, M.J. Matthews, A. V. Hamza, T. Zhu, Additively manufactured hierarchical stainless steels with high strength and ductility, Nat. Mater. 17 (2018) 63–70, https://doi.org/10.1038/nmat5021.

[28] F. Khodabakhshi, M.H. Farshidianfar, A.P. Gerlich, M. Nosko, V. Trembošová, A. Khajepour, Effects of laser additive manufacturing on microstructure and crystallographic texture of austenitic and martensitic stainless steels, Addit. Manuf. 31 (2020) 100915, https://doi.org/10.1016/j.addma.2019.100915.

[29] N. Chen, G. Ma, W. Zhu, A. Godfrey, Z. Shen, G. Wu, X. Huang, Enhancement of an additive-manufactured austenitic stainless steel by post-manufacture heat-treatment, Mater. Sci. Eng. A 759 (2019) 65–69, https://doi.org/10.1016/j.msea.2019.04.111.

[30] D. Kong, C. Dong, X. Ni, L. Zhang, J. Yao, C. Man, X. Cheng, K. Xiao, X. Li, Mechanical properties and corrosion behavior of selective laser melted 316 L stainless steel after different heat treatment processes, J. Mater. Sci. Technol. 35 (2019) 1499–1507, https://doi.org/10.1016/j.jmst.2019.03.003.

[31] P. Bajaj, A. Hariharan, A. Kini, P. Kürnsteiner, D. Raabe, E.A. Jägle, Steels in additive manufacturing: a review of their microstructure and properties, Mater. Sci. Eng. A 772 (2020) 138633, https://doi.org/10.1016/j.msea.2019.138633.

[32] M. Yang, R.D. Sisson, Carburizing heat treatment of selective-laser-melted 20MnCr5 steel, J. Mater. Eng. Perform. 29 (2020) 3476–3485, https://doi.org/10.1007/s11665-020-04564-9.

[33] C.V. Funch, K. Somlo, T.L. Christiansen, M.A.J. Somers, Thermochemical post-processing of additively manufactured austenitic stainless steel, Surf. Coat. Technol. 441 (2022) 128495, https://doi.org/10.1016/j.surfcoat.2022.128495.

[34] R. Montanari, A. Lanzutti, M. Richetta, J. Tursunbaev, E. Vaglio, A. Varone, C. Verona, Plasma carburizing of laser powder bed fusion manufactured 316 L steel for enhancing the surface hardness, Coat 12 (2022) 258, https://doi.org/10.3390/coatings12020258.

[35] M. Marinelli, E. Milani, M. Montuori, A. Paoletti, P. Paroli, J. Thomas, High-quality diamond grow by chemical-vapor deposition: improved collection efficiency in α-particle detection, Appl. Phys. Lett. 75 (1994) 3216, https://doi.org/10.1063/1.125282.

[36] B.D. Cullity, Elements of X-Ray Diffraction, second ed., Addison Wesley Publishing Company INC., Reading, Massachussets, 1977.

[37] N. Ridley, H. Stuart, Partial molar volumes from high-temperature lattice parameters of iron–carbon austenites, Met. Sci. J. 4 (1970) 219–222, https://doi.org/10.1179/msc.1970.4.1.219.

[38] S. Prawer, R.J. Nemanich, Raman spectroscopy of diamond and doped diamond, Philos. Trans. R. Soc. A 362 (2004) 2537, https://doi.org/10.1098/rsta.2004.1415.

[39] J. Robertson, Diamond-like amorphous carbon, Mater. Sci. Eng. R 37 (2002) 129–281, https://doi.org/10.1016/S0927-796X(02)00005-0.

[40] S. Kaciulis, A. Mezzi, P. Soltani, T. de Caro, H. Xia, Y.L. Wang, T. Zhai, M. Lavorgna, Reduction of graphene oxide by UHV annealing, Surf. Interface Anal. 50 (2018) 1089–1093, https://doi.org/10.1002/sia.6424.

[41] A. Mezzi, S. Kaciulis, Surface investigation of carbon films: from diamond to graphite, Surf. Interface Anal. 42 (2010) 1082–1084, https://doi.org/10.1002/sia.3348.

[42] S. Das, M.J. Hendry, Application of Raman spectroscopy to identify iron minerals commonly found in mine wastes, Chem. Geol. 290 (2011) 101–108, https://doi.org/10.1016/j.chemgeo.2011.09.001.

[43] A. Lanzutti, E. Marin, K. Tamura, T. Morita, M. Magnan, E. Vaglio, F. Andreatta, M. Sortino, G. Totis, L. Fedrizzi, High temperature study of the evolution of the Tribolayer in additively manufactured AISI 316L steel, Addit. Manuf. 34 (2020) 101258, https://doi.org/10.1016/j.addma.2020.101258.

[44] D.P. Almond, P.M. Patel, Photothermal Science and Techniques, Chapman & Hall, London, 1996.

[45] B. Jönsson, S. Hogmark, Hardness measurements of thin films, Thin Solid Films 114 (1984) 257–269, https://doi.org/10.1016/0040-6090(84)90123-8.

[46] R. Montanari, A. Sili, G. Costanza, Improvement of the fatigue behaviour of an Al6061/20%SiCp composite by means of titanium coatings, Compos. Sci. Technol. 61 (2001) 2047–2054, https://doi.org/10.1016/S0266-3538(01)00102-6.

[47] G. Costanza, R. Montanari, F. Quadrini, A. Sili, Influence of Ti coatings on the fatigue behaviour of Al-matrix MMCs. Part I: Experimental analysis, Compos. B 36, 2005, pp. 439–445, https://doi.org/10.1016/j.compositesb.2004.12.001.

[48] A.W. Zia, New generation carbon particles embedded diamond-like carbon coatings for transportation industry, in: A.S.H. Makhlouf, N.Y. Abu-Thabit (Eds.), Advances in Smart Coatings and Thin Films for Future Industrial and Biomedical Engineering Applications, Elsevier, 2020, pp. 307–332, https://doi.org/10.1016/B978-0-12-849870-5.00004-5.

[49] R. Brescia, M. Schreck, S. Gsell, M. Fischer, B. Stritzker, Transmission electron microscopy study of the very early stages of diamond growth on iridium, Diamond Relat. Mater. 17 (2008) 1045–1050, https://doi.org/10.1016/j.diamond.2008.01.115.

[50] C.S. Wang, H.C. Chen, H.F. Cheng, I.N. Lin, Growth behavior of nanocrystalline diamond films on ultrananocrystalline diamond nuclei: the transmission electron microscopy studies, J. Appl. Phys. 105 (2009) 124311, https://doi.org/10.1063/1.3153957.

[51] X.J. Li, L.L. He, Y.S. Li, Q. Yang, Revealing the nucleation mechanism of diamond film deposited on steel by high resolution transmission electron microscopy, Diamond Relat. Mater. 92 (2019) 100–108, https://doi.org/10.1016/j.diamond.2018.12.021.

[52] Y. Lifshitz, T. Köhler, T. Frauenheim, I. Guzmann, A. Hoffman, R.Q. Zhang, X. Zhou, S.T. Lee, The mechanism of diamond nucleation from energetic species, Science 297 (2002) 1531–1535, https://doi.org/10.1126/SCIENCE.1074551.

[53] X.J. Li, L.L. He, Y.S. Li, Q. Yang, Diamond deposition on Iron and steel substrates: a review, Micromachines 11 (2020) 719, https://doi.org/10.3390/mi11080719.

[54] F. Xu, J.H. Xu, M.F. Yuen, L. Zheng, Adhesion improvement of diamond coatings on cemented carbide with high cobalt content using PVD interlayer, Diamond Relat. Mater. 34 (2013) 70–75, https://doi.org/10.1016/j.diamond.2013.01.012.

[55] Y.S. Li, F. Ye, J. Corona, M. Taheri, C. Zhang, M. Sanchez-Pasten, Q. Yang, CVD deposition of nanocrystalline diamond coatings on implant alloy materials with CrN/Al interlayer, Surf. Coat. Technol. 353 (2018) 364–369, https://doi.org/10.1016/j.surfcoat.2018.07.108.

[56] X. Li, J. Chen, J. Ye, T. Feng, X. Hu, Low-stress diamond films deposited on stainless steel by a two-step dropped power process in chemical vapor deposition, Diamond Relat. Mater. 81 (2018) 176–182, https://doi.org/10.1016/j.diamond.2017.12.010.

[57] T. Morita, Y. Hirano, K. Asakura, T. Kumakiri, M. Ikenaga, C. Kagaya, Effects of plasma carburizing and DLC coating on friction-wear characteristics, mechanical properties and fatigue strength of stainless steel, Mater. Sci. Eng. A Volume 558 (2012) 349–355, https://doi.org/10.1016/j.msea.2012.08.011.